# Accepted Manuscript

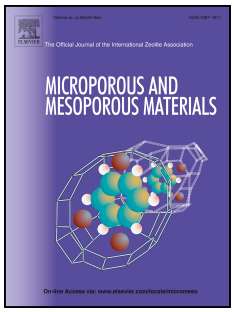


Novel Approach to the Characterization of the Pore Structure and Surface Chemistry of Porous Carbon with Ar, $N_2$, $H_2O$ and $CH_3OH$ Adsorption

C. Fan, V. Nguyen, Y. Zeng, P. Phadungbut, T. Horikawa, D.D. Do, D. Nicholson

PII: S1387-1811(15)00025-6

DOI: 10.1016/j.micromeso.2015.01.013

Reference: MICMAT 6938

To appear in: *Microporous and Mesoporous Materials*

Received Date: 7 May 2014

Accepted Date: 5 January 2015

Please cite this article as: C. Fan, V. Nguyen, Y. Zeng, P. Phadungbut, T. Horikawa, D.D. Do, D. Nicholson, Novel Approach to the Characterization of the Pore Structure and Surface Chemistry of Porous Carbon with Ar, $N_2$, $H_2O$ and $CH_3OH$ Adsorption, *Microporous and Mesoporous Materials* (2015), doi: 10.1016/j.micromeso.2015.01.013.

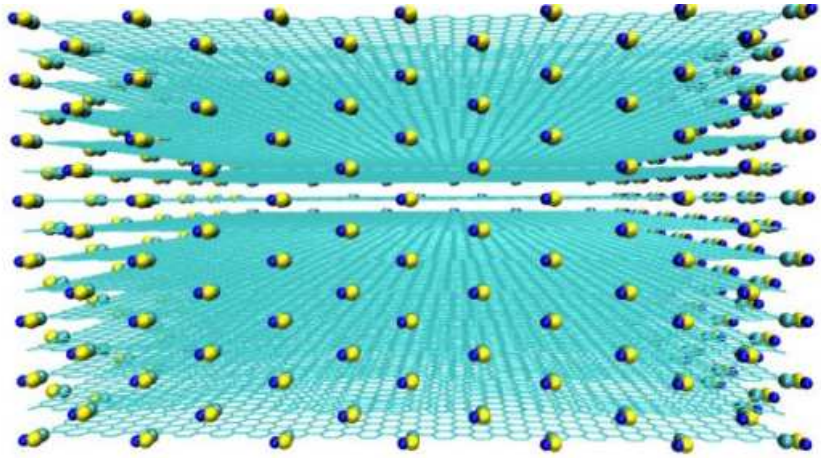

# Novel Approach to the Characterization of the Pore Structure and Surface Chemistry of Porous Carbon with Ar, $N_2$, $H_2O$ and $CH_3OH$ Adsorption

C. Fan[1], V. Nguyen, Y. Zeng, P. Phadungbut, T. Horikawa[2] D. D. Do* and D. Nicholson
School of Chemical Engineering, University of Queensland, QLD 4072, Australia
[1]Department of Chemical Engineering, Curtin University, Bentley, WA 6845, Australia
[2]Department of Advanced Materials, University of Tokushima, Tokushima, Japan

## Abstract

Characterization of porous carbon for its pore size distribution is traditionally carried out with simple pore models of well-defined geometry (slit or cylinder) with both ends opened to the gas surroundings. These idealised models do not adequately describe the inherently complex structure of porous carbons. An improved model should be sufficiently simple, not only for characterization, but also for the design of separation and purification processes. The following factors should be included: (1) energetic variation along the pore axis due to constrictions or strong energy sites, (2) connectivity between adjacent pores and (3) the presence of functional groups. In this work, we report results from computer simulations, using argon and nitrogen as non polar or weakly polar adsorbates and water and methanol as examples of associating fluids. The new model is able to produce all hysteresis loops classified by the IUPAC as well as loop types reported earlier by de Boer [1], Experimental isotherms are commonly measured at 77K and 87K (nitrogen and argon boiling points, respectively), but in recent years cryostats have become increasingly available in characterization laboratories and our simulations show that by measuring isotherms at different temperatures new insights about the porous structure can be gained from the variation of the hysteresis loop with respect to temperature which may change, for example, from a single-loop to a double-loop via a fused-loop as the temperature is varied.

* Author to whom all correspondence should be addressed. Email: d.d.do@uq.edu.au

## 1. Introduction

The characterization of porous solids has remained a subject of intense study in the last few decades. Among the many experimental methods that are available [2], the most practical (and the simplest) one for pore characterization is based on adsorption of simple gases [3], among which Ar and $N_2$ are the most commonly used. Molecular simulation has increasingly replaced classical theories because it provides an accurate solution to the statistical mechanical problem and therefore a coherent framework for pore size distribution (PSD) and its derivatives. No matter whether molecular simulation or classical theory is employed, the common denominator is the construction of a pore model. For example, the most commonly used pore model for activated carbon (AC) is the slit pore with homogeneous graphitic walls of infinite extent. However, due to the inherent heterogeneity of pore structures in AC, this simple model is clearly too elementary. Many alternative models have been proposed to account for various factors, such as surface heterogeneity [4-8], functional groups [9, 10], pore geometry [11] and finite dimensions [12]. These modifications help to improve the fit between theoretical results and experimental isotherms, and to understand the extent of this improvement it is important to study how each of the above factors affects the adsorption isotherm. This is the main aim of this paper.

A significant feature of the adsorption isotherms for mesoporous solids is the hysteresis loop. An early proposal to classify hysteresis loops in terms of porous structure were put forward by de Boer (dB) [1] who introduced the five types shown in Figure 1. Later, the IUPAC identified four loop types (H1 to H4) based on experimental isotherms observed for disordered solids [13], which are shown in Figure 2. The H1 and H2 Types correspond to Types A and E in the dB classification, while H3 and H4 are associated with slit-like pores. Curiously, some of the loop types suggested by de Boer were omitted in the IUPAC classification, and this is probably due to the limited topologies of porous structure in real disordered solids. With the recent surge in the synthesis of new materials, especially ordered mesoporous solids, for example MCM-41 [14] and SBA-15 [15], many different hysteresis loops have been observed, including Type C of de Boer [16, 17] and a type mixed between Type H1 and Type C [18, 19].

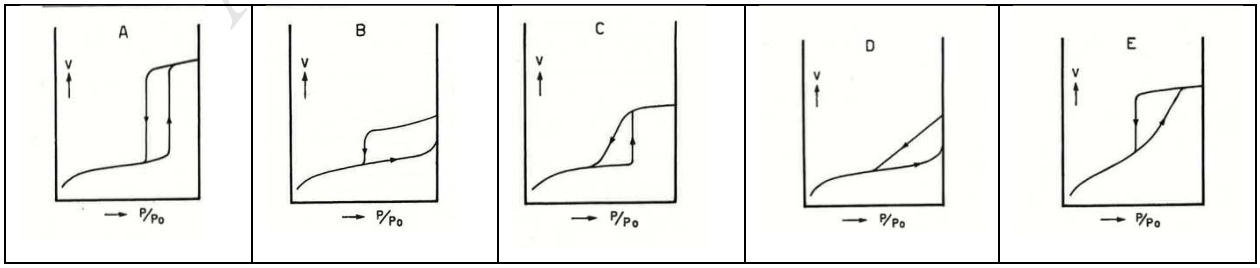


**Figure 1**: de Boer classification of hysteresis [1]

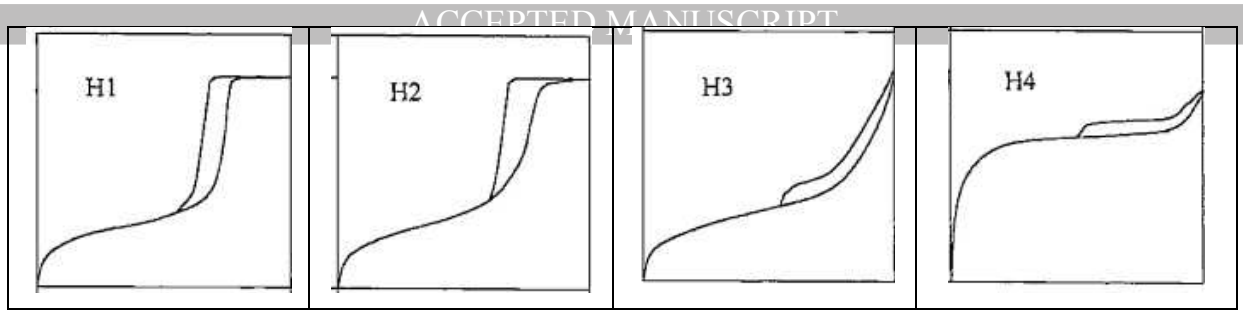


**Figure 2**: IUPAC classification of hysteresis [13].

Adsorption of non-polar gases to characterize the porous structure of a solid is common, but a full characterization for the purpose of adsorptive separation and purification of mixtures involving polar fluids, especially associating fluids, requires the determination of the surface chemistry. The effects of the surface chemistry on adsorption have been illustrated by Bandosz and co-workers [20-24]. They found that adsorption of water is very sensitive to surface heterogeneity but the physical structure has limited effects in the low pressure region. Similar conclusions were also drawn by Thommes et al. [25, 26], who proposed water as a probe to characterize the surface chemistry of carbon materials.

The structure of this paper is as follows: in Section 2, the simulation method and the potential models are presented, and various basic pore models are described. In Section 3, the results from simulations of adsorption in these models are discussed, with particular attention to the use of non-polar argon as an adsorbate in Sections 3.1 to 3.6, and to water and methanol as representatives of associating fluids, in Section 3.7 as a probe for the nature of functional groups. Conclusions drawn from this study are presented in Section 4.

## 2. Theory and Simulation

### 2.1 Interaction Energy

The intermolecular potential energy is described by the combination of the 12-6 Lennard-Jones (LJ) equation and the Coulombic equation. The molecular parameters of the adsorbates and for the phenol group are summarized in Table 1.

**Table 1:** Molecular Parameters for potential models of argon, nitrogen, methanol, water and phenol group.

| | Site | x(nm) | y(nm) | z(nm) | σ(nm) | $\varepsilon/k_B$(K) | charge(e) |
|---|---|---|---|---|---|---|---|
| Ar [27] | Ar | 0 | 0 | 0 | 0.3405 | 119.8 | — |
| $N_2$ [28] | $N_2$ | 0 | 0 | 0 | 0.36154 | 101.5 | — |
| $CH_3OH$ [29] | $CH_3$ | -0.143 | 0 | 0 | 0.375 | 98.0 | 0.265 |
| | O | 0 | 0 | 0 | 0.302 | 93.0 | -0.7 |

| | | | | | | | |
|---|---|---|---|---|---|---|---|
| | H | 0.0299853 | 0.08962 | 0 | — | — | 0.435 |
| | O | 0 | 0 | 0 | 0.3166 | 78.205 | -0.8476 |
| $H_2O$ [30] | H1 | -0.0816490 | 0.0577359 | 0 | — | — | 0.4238 |
| | H2 | -0.0816490 | 0.0577359 | 0 | — | — | 0.4238 |
| | C[a] | 0 | 0 | 0 | — | — | 0.2 |
| -C[a]-OH [30] | O | 0 | 0.1364 | 0 | 0.307 | 78.2 | -0.64 |
| | H | 0.0899205 | 0.1700220 | 0 | — | — | 0.44 |

[a] Carbon located in the plane of a graphene sheet.

For slit pores of infinite extent in the directions parallel to the pore walls, the Steele 10-4-3 equation [31] is used to calculate the solid-fluid (SF) potential energy, with the following parameters: $\sigma_{ss} = 0.34nm$, $\varepsilon_{ss}/k_B = 28K$ and $\rho_s = 38.2nm^{-2}$ for a graphene layer, where $\sigma_{ss}$ and $\varepsilon_{ss}$ are the collision diameter and the well depth of pairwise interaction of carbon atoms and $\rho_s$ is the surface density of solid atoms. For slit pores which are finite in one direction and infinite in the other direction (parallel to the pore walls), the Bojan-Steele equation [32-34] is used; each pore wall consists of three graphene layers with an interlayer spacing of 0.3354nm. The cross collision diameter and well-depth of the solid-fluid interaction energy were calculated by the Lorentz-Berthelot mixing rule.

### 2.2 Pore Models

The schematics of the pore models are presented in Figure 3, with the finite pore of uniform pore width used as the reference for the subsequent comparison with other models. The length of the simulation box in the x-direction was 10 times the collision diameter of the fluid, and the lengths for the other two directions were determined by the pore dimensions. Mechanical equilibrium between the adsorbate inside the pore and the surroundings was established by connecting a gas reservoir at the pore opening with a length of 3nm along the pore axis (which has been shown to be sufficient to model the gas phase since larger reservoirs give the same results), and the same dimensions in the other two directions as those of the pore. Variants of the basic pore model are as follows:

(1) to study the effects of a closed end (often referred to as dead end pores) we added a graphitic wall at one end of the finite slit pore (Figure 3b),
(2) to study the variation in the pore size along the pore axis we consider five models;
    a. a pore with two distinct sections, each of uniform pore size (Figure 3c),
    b. an ink-bottle pore in which a large cavity is connected to the surroundings through a smaller neck (Figure 3d),
    c. a pore in which pore width varies linearly along the pore axis, known as a wedge pore (Figure 3e),

d. a pore with constrictions along the pore axis (Figure 3f), and
e. a model that accounts for the presence of functional groups; constructed by grafting the groups randomly at the edge of a finite slit pore (Figure 3g).

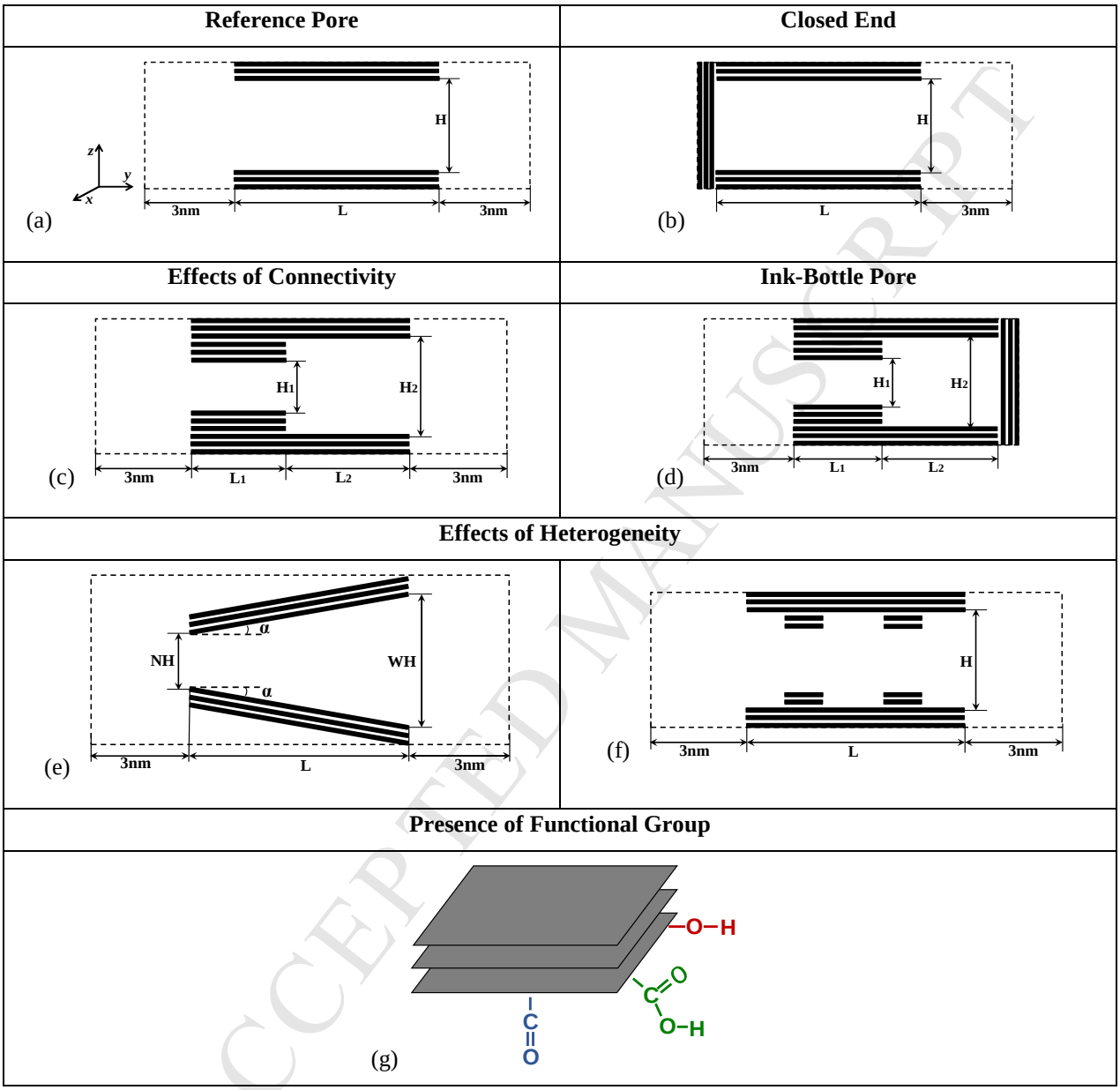


**Figure 3:** The schematics of the pore (solid) models examined in this work, (a) open slit pore, (b) closed end pore, (c) connected pore, (d) ink-bottle pore, (e) wedge pore, (f) corrugated pore, (g) graphene layers with functional groups attached at the edge.

## 2.3 Simulation Method

GCMC simulation was used to obtain adsorption isotherms, with 100,000 cycles for the equilibration stage and the same number for the sampling stage. Each cycle consists of 1000 displacement moves and exchanges (insertion and deletion), with equal probability. In the

equilibration stage, the maximum displacement length was initially set as half of the largest dimension of the box and was adjusted at the end of each cycle to give an acceptance ratio for displacement of 20% [35, 36]. For the infinite pore, periodic boundary conditions were applied at the boundaries in the *x*-and *y*- directions, while for the finite pore it was only applied in the *x*-direction, and the cut-off radius was 5 times the collision diameter (half of the simulation box dimension along the direction of infinite extent).

## 3. Results and Discussion

### 3.1 Simple Slit Pore

3.1.1. Infinite pore vs. finite pore length

The implication of a pore of infinite extent is that when the pore is filled the condensed adsorbate is an infinite column of liquid-like phase (or solid-like phase if the temperature is well below the triple point), and therefore when the pressure is decreased desorption occurs via a cavitation process because of the absence of a pore opening. For finite pores connected to the gas surroundings, a gas-liquid interface is formed at the pore mouth and during desorption it recedes into the pore interior as the pressure is decreased. Transfer of molecules from the interior to the surrounding occurs across this interface; a process of which makes desorption from a finite pore distinctly different from an infinite pore, no matter how long the finite pore is [37]. The effects of length on adsorption are not new, but for the sake of completeness in the discussion of various pore models we have highlighted the key differences in Figure 4 for adsorption isotherms of Ar at 87K in slit pores with two open ends. Three points may be emphasised:

(a) The hysteresis loop is type H1 regardless of the pore length, except for very short pores whose isotherms are reversible.

(b) As the pore length is increased, the condensation pressure shifts to a lower value and approaches the condensation pressure of the infinitely long pore because of the greater solid-fluid interaction, and the evaporation pressure also shifts to a lower value but never approaches the evaporation pressure of the infinitely long pore. This is a consequence of the two distinct mechanisms for evaporation in the finite pore and the infinitely long pore as elaborated above.

(c) The fact that the condensation pressure shifts to a higher pressure for a finite pore, relative to the corresponding infinite pore, has a significant implication in the determination of pore size. If a pore model of infinite length is used for the characterization of a solid having pores of

finite length, the pore size would be overestimated as has been recently recognized in the literature [38].

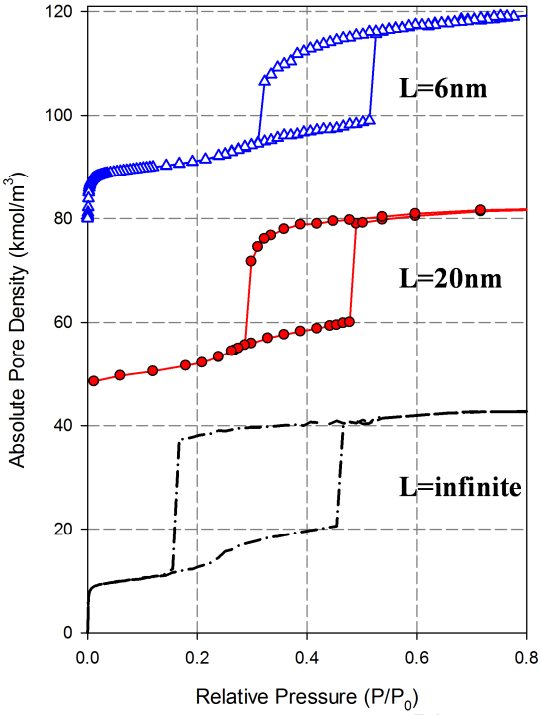


**Figure 4 :** The comparison of the adsorption isotherm of argon at 87K in the slit pore with infinite and finite pore lengths, the pore width is 3nm the length of the pores are as marked in the figures.

### 3.1.2. Open end vs. closed end

Porous carbon materials have a wide distribution of pore size, ranging from micropores to mesopores, and they are intertwined in a complex manner. However, no matter how complex this is, micropores behave as open end pores and are filled reversibly at very low pressures; after that has occurred the adjacent mesopores will behave as closed end pores. In this section we shall highlight the differences between the behaviour of an open end pore and a closed end pore. The most debatable point is whether isotherms for closed end pores are reversible, or whether they can exhibit hysteresis. According to the classical theories based on the Kelvin-Cohan equation, the isotherm must always be reversible in a closed end pore because the same shape of interface separates the gas phase and the adsorbed phase in both adsorption and desorption. However, our extensive simulation results have shown that, under certain conditions, hysteresis is possible. The reasons for the failure of classical theories to predict hysteresis are that: (1) they do not account for the progressive structural change of the adsorbed phase with the extent of adsorption and (2) they do not account for the difference in the thickness of the adsorbed layer, which is metastable in adsorption but is close to a stable state in desorption [39, 40].

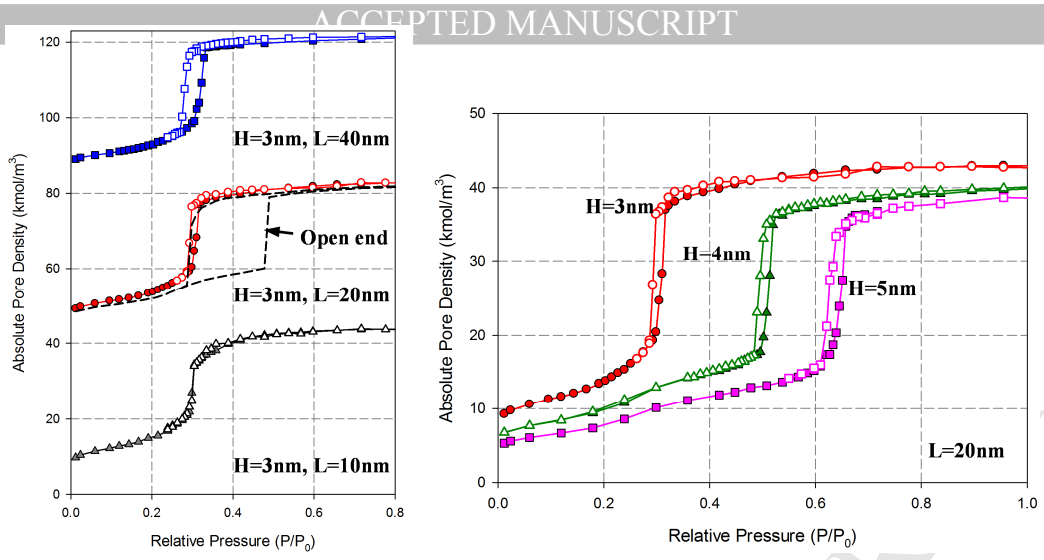


(a) (b)

**Figure 5:** Argon adsorption at 87K in slit pores with uniform width, (a) isotherms for closed end pores with widths 3nm and different pore lengths The isotherm of the open end pore with 20nm length is presented by a dashed line for comparison; (b) isotherms for closed end pores of 20nm length and different widths.

To show how the presence of a closed end can affect the isotherm, and the impact on the characterization of a porous solid, we presented in Figure 5a the adsorption isotherms (the set in the middle of the figure) in two slit pores of 3nm width and 20nm length, one of which has open ends and the other with one end closed. It can be seen that the presence of the closed end changes the adsorption behaviour significantly: (1) although the hysteresis loop remains Type H1, its size is much smaller, (2) the condensation and evaporation are not gradual, but very sharp, and the onset of condensation as well as evaporation occurs at lower pressure, with a greater shift in the condensation, resulting in a smaller loop. These features are again observed for other dimensions of closed end pores, except for short pores whose isotherms are reversible. This is seen in Figures 5a and b where we show the effects of pore length and width. The hysteresis loop is larger for longer pores with the condensation shifting to larger pressure and the evaporation shifting to lower pressure. For larger pore widths the loop shifts to higher pressure but retains the same shape and size.

### 3.2 Effects of Connectivity

In porous carbons, the variability in pore shape and the interconnections among pores are too complex to be described adequately by simulation. However, we can illustrate the essential features of connectivity by considering a simple connected pore with two adjacent sections of uniform size with two ends open to the gas surroundings (Figure 3c). This is simple model is sufficient to show how the behaviour of an adjacent pore can affect adsorption and desorption of a given pore. Figure

6 shows the adsorption isotherm for a connected pore with widths of 3 nm and 3.68 nm for the two sections, both of length 6nm. The behaviour of this connected pore is different from that of the isolated uniform pores of 3nm and 3.68nm. The first distinction is the shape of the hysteresis loop. It changes from Type H1 to Type C of de Boer, and this is typical of an open end pore with non-uniform pore size in the axial direction (we will see this behaviour again when we deal with wedge pore later). The Type C hysteresis loop is characterized by vertical condensation and gradual evaporation. The reason for the single stage condensation is that the widths of the two sections are not very different; when condensation has occurred in the smaller section there is an avalanche effect which induces a condensation in the larger section. This occurs because the radius of curvature of the interface after the condensation in the smaller section is larger than the half width of the larger section, giving rise to an instant condensation of the larger section whatever its length. This mechanism has a significant implication for the characterization of a porous solid having similar connectivity. If one uses the condensation pressure to determine the pore size by using kernels calculated for open end pores, one would underestimate the pore size by an extent that increases with the length of the larger section. This observation highlights the need to construct kernels derived from various elementary pore models as a basis for the determination of pore size distribution. The discrimination among these kernels, or their combination, will require supplementary experimental data and further analysis; for example by measuring isotherms at different temperatures.

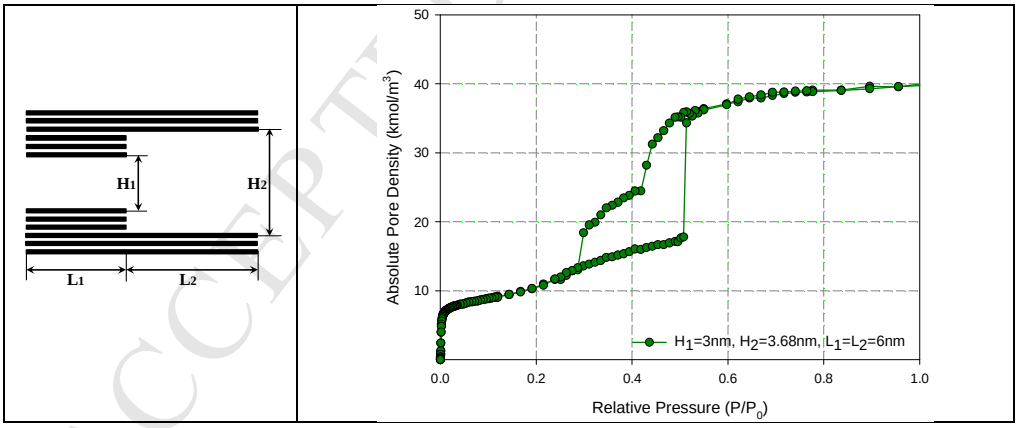


**Figure 6:** Isotherms for argon adsorption at 87K in connected slit pores with two open ends, the widths of the narrow and wide pores are 3nm and 3.68nm, respectively, and the length for each is 6nm.

A further example of the implications of connectivity is illustrated in Figure 7a which shows the isotherms for the isolated two open end pores having the same widths as the two sections of the connected pore in Figure 6, and the isotherm for a closed end pore having the same width as the larger section. From these isotherms we constructed two combined isotherms: (1) using the isotherms of two open end pores and (ii) using the isotherm of open end pore of smaller width and

that of the closed end pore of larger width. These combined isotherms are shown in Figure 7b and may be compared with the isotherm for the connected pore, also shown in the same figure. The first combined isotherm, using two open end pores, is a poor match for the isotherm for the connected pore, while the second one gives much closer description. This finding implies that by analysing the adsorption branch to determine the pore size distribution (PSD) using a kernel of pores with open ends, we would obtain a single pore size equal to that of the smaller pore. On the other hand, if we use the desorption branch, we would underestimate the pore size because the evaporation from the connected pore occurs at a lower pressure than from the two uniformly sized pores. This again calls into question the reliability of characterizations based on a single isotherm for the determination of PSD.

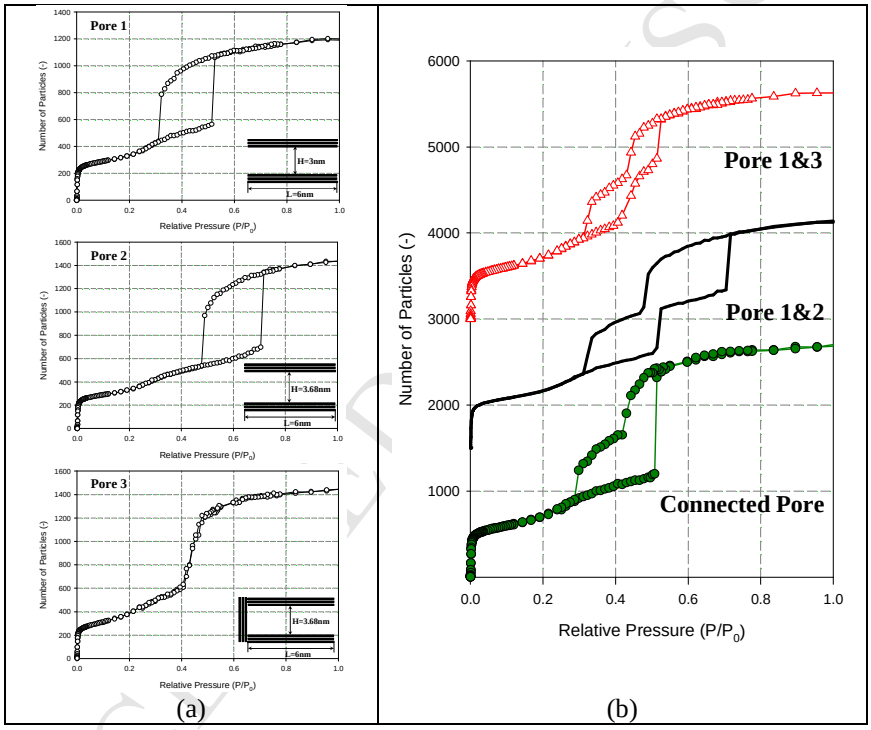


**Figure 7:** Isotherms for argon adsorption at 87K in slit pore with two open ends, (a) the unit cells that comprised the connected pore in Figure 6, (b) comparison between the connected pore and the combined isotherms based on unit cells.

### 3.3 Cavitation and Pore Blocking

The ink-bottle pore is a model that combines two of the features that we just discussed: pores with a closed end and connectivity, and the model is commonly used to explain two alternative mechanisms of evaporation: cavitation and pore blocking. Figure 8 shows a series of isotherms for argon adsorption at 87K in ink-bottle pores with different neck widths. When the neck has the same width as the cavity, this pore is a closed end pore of uniform size and its hysteresis loop is Type H1,

as discussed in Section 3.1.2. When the neck width is reduced new features appear as summarized below:

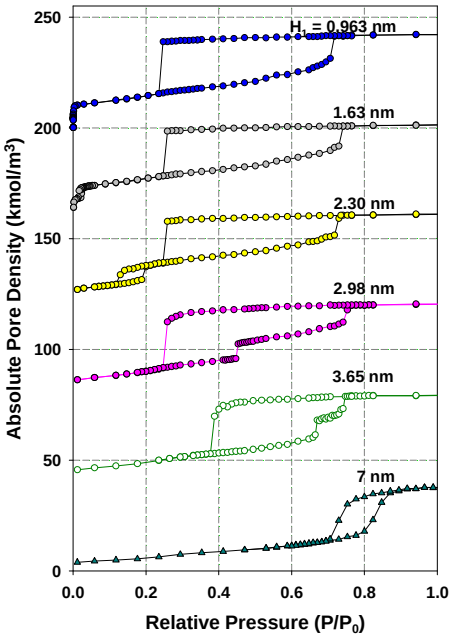


**Figure 8:** Isotherms for argon adsorption at 87K in Ink-bottle pores, the dimensions of the cavity are 7nm × 7nm, and the neck length is 10nm, the widths of the necks are as labelled in the graph.

(i) When the neck size is smaller than a critical size, which is around 3nm, the cavity is emptied via cavitation; exhibited as a steep evaporation at a reduced pressure of 0.24. The neck is emptied at the same pressure as for this critical neck size or at lower pressures for neck sizes that are smaller than the critical value.

(ii) When the neck size is greater than the critical size, the evaporation occurs at a higher pressure than the cavitation pressure, indicating a change in the evaporation mechanism from cavitation to pore blocking [41].

More details about the adsorption behaviour for ink-bottle pore can be found in references [41, and 42].

### 3.4 Effects of Heterogeneity

#### 3.4.1 Wedge Pore

The wedge pore has been studied as a further example of pores with a non-uniform cross section. Adsorption in pores of this type is similar to that in connected pores, discussed in Section 3.2. The isotherm for a wedge pore has a Type C (in the dB scheme) hysteresis loop whose detailed shape depends on the width of the narrow end and the angle of the wedge (see Figure 9). The reason that Type C hysteresis is not commonly observed experimentally is that wedge configurations are

masked by other effects, such as closed ends and ink-bottle structures, and may be the principle reason why it was rejected in the IUPAC classification of 1985. A new IUPAC classification, presented in the COPS-X meeting, addresses this deficiency and proposed that Type C should be designated as Type H2b, with the original H2 being re-classified as H2a. More details of the isotherms for wedge pores can be found in Fan et al. [43], where these and also pores with curved walls are studied.

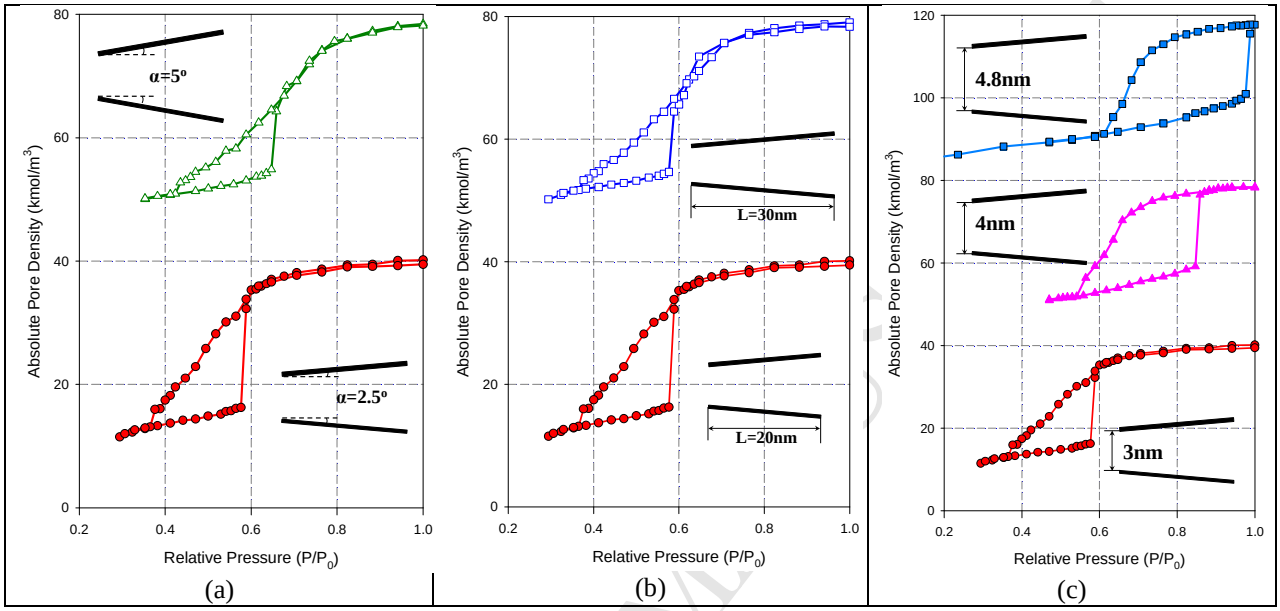


**Figure 9:** Argon adsorption isotherms at 87K in open slit pore with wedge shapes, (a) the width of the narrow end is 3nm, the axial length is 20nm and the wedge angles are $5^o$ and $25^o$; (b) the width of narrow end is 3nm, the wedge angle is 2.5° and the axial length is varied; (c) the wedge angle is 2.5°, the axial length is 20nm and the widths at the narrow end are varied.

### 3.4.2 Corrugation

Pores in real materials do not have homogeneous surfaces, but possess geometrical corrugations which come from impurities or defects acquired during synthesis or arise naturally as a consequence of discrete atomic structure. We have simulated corrugation by grafting small humps of 2nm length along the pore axis onto open end pores and closed end pores (see Figure 3f). The height of the hump was chosen to be either 0.335nm or 0.67nm. Figure 10a shows the adsorption isotherm of argon at 87K in 3nm open end pores with various corrugations, together with isotherms for uniform pores (i.e. without corrugations). Figure 10b shows the corresponding isotherms for closed end pores. Even for this simple model of corrugation we observed a rich behaviour of the hysteresis loop, depending on the size of the corrugation and its spatial distribution. The hysteresis observed for the open end pore with one corrugation of 0.335nm height in the middle of the pore catches our immediate attention; it has one principle loop which is rather sharp, followed by a secondary gradual loop as pressure is decreased. This type of hysteresis loop has been observed with benzene adsorption on activated charcoals [44].

This two stage desorption process is also observed with closed end pores having one corrugation in the middle, regardless the height of the corrugation; however, the first stage is small compared to the second one.

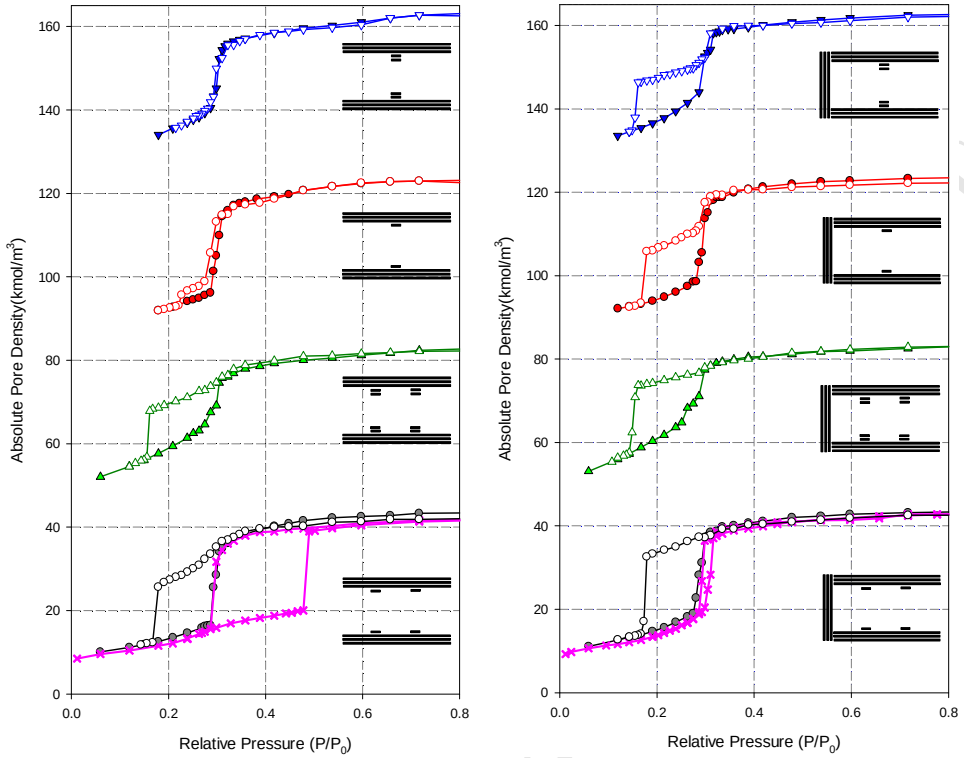


**Figure 10:** Argon adsorption isotherms at 87K in slit pore with corrugations on the pore walls, the width of the pore is 3nm and the length 20nm, (a) open end and (b) closed end. The corresponding pore structure for each isotherm is shown in the graph.

The effects of the spatial distribution of the corrugation are shown in the bottom two isotherms in Figure 10 for two equally spaced corrugations. There are two distinct, and interesting, features of the hysteresis: (1) Type H2 is observed in both open and closed end pores for 0.67nm corrugations, and (2) Type H1 for 0.335nm corrugation. The implication of these results is that experimental isotherms with H1 or H2 hysteresis could come from either open or closed end pores when there is corrugation in the pore cross section.

### 3.5 Evolution of Hysteresis with Temperature

We have mentioned earlier that the analysis of a single isotherm is not sufficient to bring out the fine features of the porous structure. It is expected that different pore structures would respond differently to temperature, and this can be exploited to gain further insight into these structures. We illustrated this point in Figure 11 for three pore models: (1) uniform slit pore with two open ends (as a reference), (2) a closed end pore and (3) a wedge shape pore. First, we discuss the temperature dependence of the hysteresis loop for a uniform open end slit pore (Figure 11a) for a range of temperature from 60 to 120K. A few points may be noted:

(i) The size of the hysteresis loop decreases with temperature, and the isotherm is reversible for temperatures greater than 120K, which is the critical hysteresis temperature for argon in a pore of 3nm width;

(ii) The adsorption branch shifts to lower reduced pressure with an increase in temperature, while the desorption shifts to higher reduced pressure;

(iii) A two-step adsorption branch is observed at 60K, with the first step due to 2D-condenstion on the pore walls, and the second one to capillary condensation.

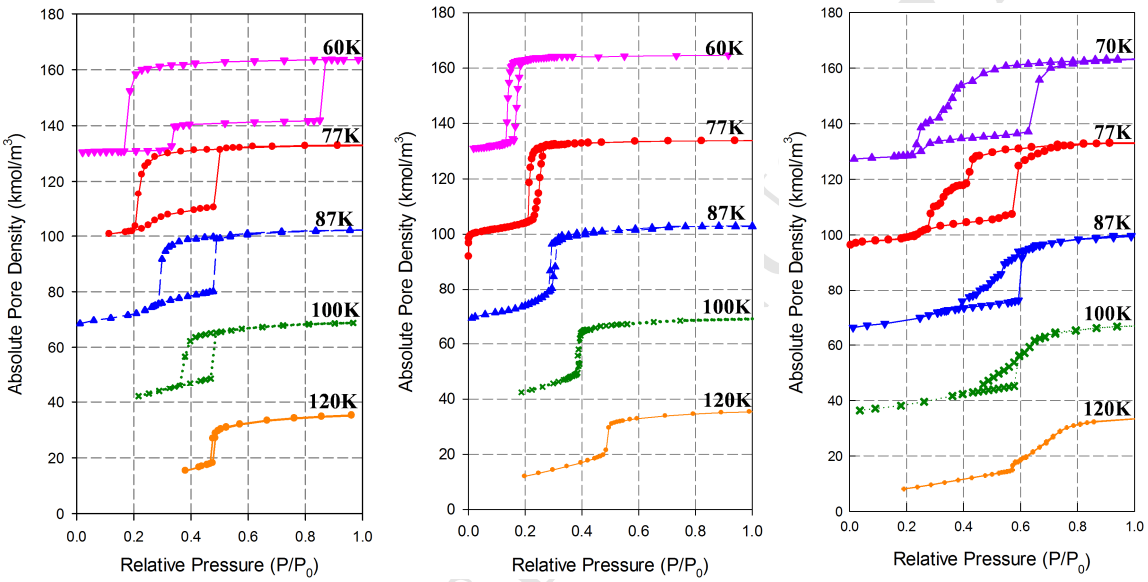


**Figure 11:** Argon adsorption isotherms at different temperatures in a slit pore with width 3nm and length 20nm, (a) open end pore, (b) closed end pore, (c) wedge shape pore with an angle of 2.5°, the saturation vapour pressure was calculated based on the equation proposed by Lotfi et al. [45].

For closed end pores, the size of the hysteresis loop also decreases with increasing temperature, and the critical hysteresis temperature is 120K (Figure 11b). In contrast to the corresponding open end pores, both the adsorption and desorption branches shift to higher reduced pressure with temperature although they both have H1 Type hysteresis. The temperature dependence of the hysteresis for the wedge pore is distinctly different from the open end and closed end pores. Not only does the hysteresis loop become smaller as temperature increases, but the shape of the loop changes from Type C to a combination of Type C and Type H1 when temperature is decreased from 100K to 70K.

The different evolution of the hysteresis loop with temperature illustrated by the above three pore models indicates that temperature is an important variable to discriminate pore models used in the characterization.

### 3.6 H3 & H4 Type of Hysteresis

H3 and H4 hysteresis loops are commonly observed for adsorption of gases on activated carbons, and a characteristic is the step down in the desorption branch at a relative pressure of 0.42 and 0.38 for nitrogen and argon respectively at their boiling points [13], in addition to the relatively flat and parallel adsorption and desorption boundaries of the hysteresis loop. None of the pore models discussed above could produce these hysteresis types for two reasons: (1) the wide distribution in pore size in activated carbon and (2) the predominant contribution of micropores compared to mesopores to the pore volume. To produce H3 and H4 there is a need to combine pore models.

We used the experimental data for Norit-CMC-2 Carbon [7] to show how different pore models can be constructed to reproduce the data. The isotherms in Figure 12a were constructed from open end pores of different sizes and are seen to give a good match to experimental data without performing any optimization. Another possibility is to combine open end pores and ink-bottle pores, as in the re-constructed isotherm shown in Figure 12b which also successfully captures the general pattern of the experimental data.

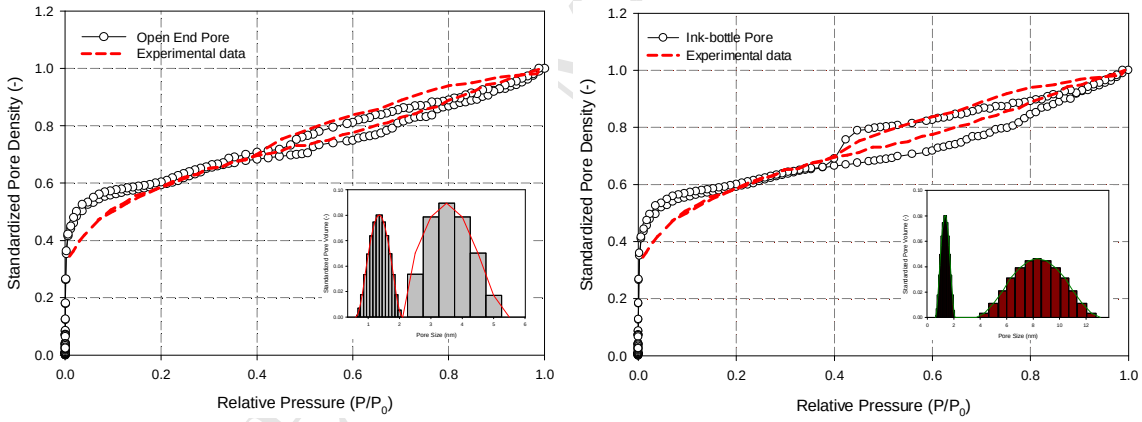


(a) (b)

**Figure 12:** Re-constructed isotherms with kernels of: (a) open end pore, (b) open end pore and ink-bottle pores, compared with experimental data for Norit-CMC-2 Carbon [7].

It is clear from the above illustration that an experimental isotherm could be captured by quite different pore models, and once again exposes the need to consider additional dimensions in characterization space; we suggest that temperature would be one possible solution to this endeavour.

### 3.7 Functional Group

In most carbonaceous materials, functional groups (oxygen-containing groups) are likely to be present on the surface, even after heat treatment at high temperature. Characterization of these

groups and their concentration is important in the modelling of adsorption of strongly polar fluids. We have shown that by using either water or methanol as adsorptives the role of functional group can be elucidated [46]. We used highly graphitized thermal carbon black (Carbopack F) as an example to show the differences between the adsorption of associating fluids and the functional group and the adsorption of simple gases (argon and nitrogen).

The role of the functional group can be clearly seen by first studying the interaction of different gases (argon, nitrogen, water and methanol) with a homogeneous graphite surface by estimating the Henry constant [46]. The Henry constant is determined by the volume integration of the Boltzmann factor over the accessible volume space [47], and is then compared with the experimental constant, which includes contributions from both the graphite surface and the functional groups. This allows us to determine not only the role of functional group, but also the relative magnitude of the fluid-fluid, fluid-graphite and fluid-functional group interactions. Figure 13 shows the simulated adsorption isotherms for the four adsorbates on Carbopack F at various temperatures, together with the corresponding experimental data. A number of points can be summarised as follows:

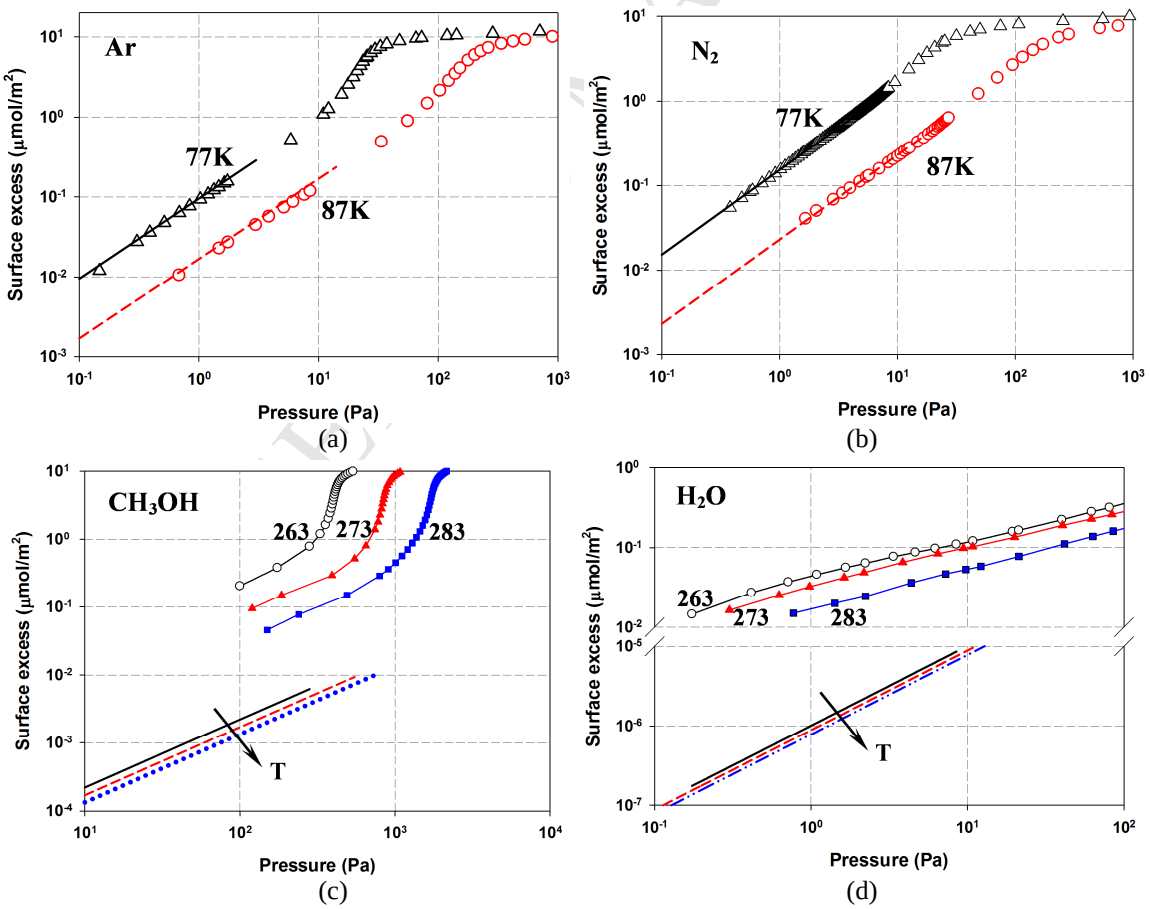


**Figure 13:** Comparison of experimental and simulated adsorption isotherms for (a) argon, (b) nitrogen, (c) methanol and (d) water on Carbopack F at different temperatures.

(i) The simulated isotherms agree well with the experimental data for non-polar gases argon and nitrogen, indicating that these adsorptives adsorb mainly on the basal planes, and there is negligible contribution from the functional groups. The Henry constants decrease with temperature, due to the exothermicity of physical adsorption.

(ii) A decrease in the Henry constant with temperature was also observed for methanol and water, but the experimental values are much higher than those calculated for the non-polar gases on the basal-plane, indicating that the initial adsorption occurs at the functional group sites.

(iii) The experimental isotherms of methanol and water are much more sensitive to temperature at low loadings than the simulation results. This is due to the greater enthalpy change caused by the adsorption on functional groups than on the graphite surface.

As well as the relative strength of interaction between adsorbate and graphite, and adsorbate and functional, the strength of adsorbate-adsorbate interactions can also be assessed by considering the modified Henry constant, $K' = KP_0$. Figure 14 shows the adsorption isotherms of methanol and water on Carbopack F plotted against the reduced pressure. Some of the interesting features observed are detailed below:

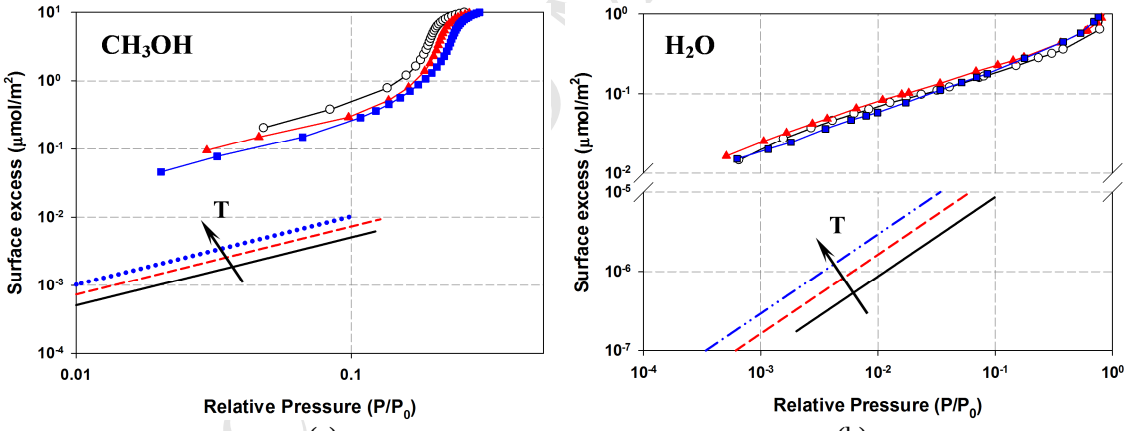


(a) (b)

**Figure 14:** Comparison of experimental and simulation adsorption isotherms of (a) methanol and (b) water on Carbopack F at different temperatures.

(i) The experimental value of the modified Henry constant for methanol decreases with temperature, but for water it is insensitive to the temperature change, this suggests the following order of interaction:

**Methanol-Functional Groups > Methanol- Methanol**

**Water-Functional Groups ≈ Water- Water**

(ii) The theoretical basal-plane based modified Henry constants for both methanol and water increase with temperature, suggesting that the intermolecular interactions are stronger than interactions between an adsorbate molecule and the basal plane.

(iii) For argon and nitrogen, the variation of the modified Henry constants with temperature are identical to that in Figures 13a and b, indicating that the interaction between the adsorbate and the basal plane is stronger than the intermolecular interactions.

It is clear that the functional group plays a very important role in the adsorption of associating fluids on carbon materials, and to this end we have recently developed a molecular model of graphite with functional groups grafted at the edges, as shown in Figure 15a (here the phenol group is used to model the functional group). With this new molecular model, the experimental data for water on a graphite surface has been re-produced correctly for the first time, as shown in Figure 15b. This also allows us to elucidate the mechanism of water adsorption: water molecules mainly cluster around the functional group, rather than on the basal plane, and once water has been adsorbed on the functional group, this complex acts as a nucleus for more water molecules to grow around it and form a larger cluster because the water-water intermolecular interaction is much greater than that between water and the basal plane. More details can be found in [48].

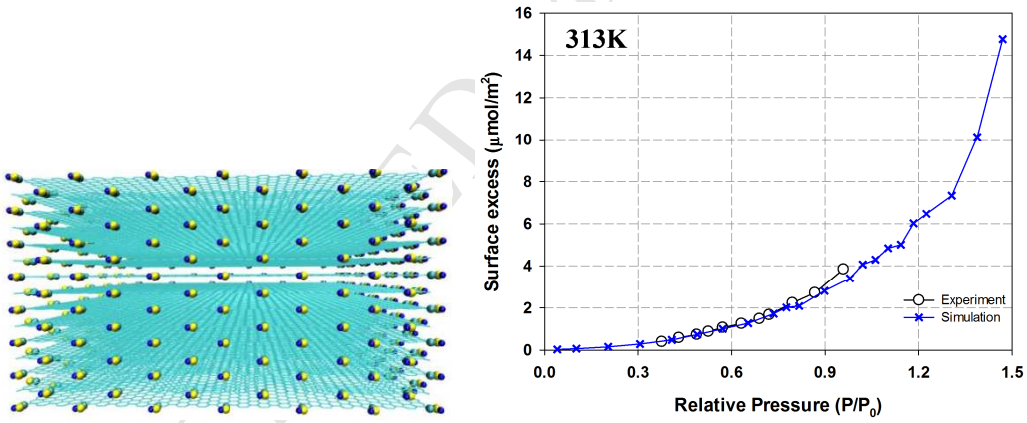


(a) (b)

**Figure 15:** (a) The side view of the graphene model with phenol groups attached at the edge; (b) the adsorption isotherm of water on graphitized carbon black at 313K obtained from the new model and compared with experimental data.

## 4. Conclusions

This paper presents a wide-ranging discussion of the characterization of physical structure and surface chemistry in porous solids based on comprehensive computer simulations carried out in our laboratory over the last 10 years. Non-polar gases (argon and nitrogen) have been used to characterize porous structure using pore models that account for finite size, closed end, variation in pore size, and corrugation in the pore width. These models represent a significant advance over the simple models with uniform pore size and two ends open to the gas surroundings frequently used as a basis for pore size distribution calculations. With these new models, all type of hysteresis loop observed experimentally can be reproduced, and we suggest that by using temperature as a variable it should be possible to delineate the relative contributions of these pore models in a given solid.

We have shown how water and methanol can be used as the probe to determine the concentration of functional groups, and with the procedure presented in this paper we can determine the relative interactions between fluid-solid, fluid-fluid and fluid-functional groups. To characterize adsorption of an associating fluid on a carbon surface, we have proposed a molecular model in which functional groups are grafted at the edges of the graphene layers, and this model is shown to be successful in describing water adsorption on graphitized carbon black over a range of temperatures.

## Acknowledgement

The financial support by the Australian Research Council to this project is acknowledged.

## References


[1] J.H. De Boer, The structure and texture of a physical adsorbent, Colloques Internationaus du CNRS, 201 (1972) 407.

[2] H. Marsh, F. Rodriguez-Reinoso, Activated Carbon, Elservier, Great Britain, 2006.

[3] F. Rouquerol, J. Rouquerol, K. Sing, Adsorption by powders and porous solids, Academic Press, London, 1999.

[4] J.C. Alexandre de Oliveira, R.H. Lopez, J.P. Toso, S.M.P. Lucena, C.L. Cavalcante, Jr., D.C.S. Azevedo, G. Zgrablich, On the influence of heterogeneity of graphene sheets in the determination of the pore size distribution of activated carbons, Adsorption-Journal of the International Adsorption Society, 17 (2011) 845-851.

[5] J. Jagiello, J.P. Olivier, Carbon slit pore model incorporating surface energetical heterogeneity and geometrical corrugation, Adsorption-Journal of the International Adsorption Society, 19 (2013) 777-783.

[6] P.R.G. Silvino, D.V. Goncalves, R.V. Goncalves, S.M.P. de Lucena, D.C.S. Azevedo, Strategies to Improve Pore-size Distribution Characterization of Activated Carbons using CO2 and N-2 Isotherms: Volume Regularization and Etched Slit Models, Adsorption Science & Technology, 31 (2013) 263-274.

[7] A.V. Neimark, Y. Lin, P.I. Ravikovitch, M. Thommes, Quenched solid density functional theory and pore size analysis of micro-mesoporous carbons, Carbon, 47 (2009) 1617-1628.

[8] S.K. Bhatia, Density Functional Theory Analysis of the Influence of Pore Wall Heterogeneity on Adsorption in Carbons, Langmuir, 18 (2002) 6845-6856.

[9] A. Gotzias, E. Tylianakis, G. Froudakis, T. Steriotis, Effect of surface functionalities on gas adsorption in microporous carbons: a grand canonical Monte Carlo study, Adsorption-Journal of the International Adsorption Society, 19 (2013) 745-756.

[10] S. Furmaniak, A.P. Terzyk, P.A. Gauden, P.J.F. Harris, P. Kowalczyk, Can carbon surface oxidation shift the pore size distribution curve calculated from Ar, N-2 and CO2 adsorption isotherms? Simulation results for a realistic carbon model, Journal of Physics-Condensed Matter, 21 (2009).

[11] J.P. Toso, R.H. Lopez, D.C.S. de Azevedo, C.L. Cavalcante, Jr., M.J. Prauchner, F. Rodriguez-Reinoso, G. Zgrablich, Evaluation of a mixed geometry model for the characterization of activated carbons, Adsorption-Journal of the International Adsorption Society, 17 (2011) 551-560.

[12] J. Jagiello, J.P. Olivier, A Simple Two-Dimensional NLDFT Model of Gas Adsorption in Finite Carbon Pores. Application to Pore Structure Analysis, The Journal of Physical Chemistry C, 113 (2009) 19382-19385.

[13] K.S.W. Sing, D.H. Everett, R.A.W. Haul, L. Moscou, R.A. Pierotti, J. Rouquerol, T. Siemieniewska, Reporting physisorption data for gas/solid systems with special reference to the determination of surface area and porosity (Recommendations 1984). Pure and Applied Chemistry, 57 (1985) 603-619.

[14] C.T. Kresge, M.E. Leonowicz, W.J. Roth, J.C. Vartuli, J.S. Beck, Ordered Mesoporous Molecular-Sieves Synthesized by A Liquid-Crystal Template Mechanism, Nature, 359 (1992) 710-712.

[15] D.Y. Zhao, Q.S. Huo, J.L. Feng, B.F. Chmelka, G.D. Stucky, Nonionic triblock and star diblock copolymer and oligomeric surfactant syntheses of highly ordered, hydrothermally stable, mesoporous silica structures, Journal of the American Chemical Society, 120 (1998) 6024-6036.

[16] M. Kruk, J.R. Matos, M. Jaroniec, Argon and nitrogen adsorption studies of changes in connectivity of ordered cage-like large mesopores during the hydrothermal treatment, Colloids and Surfaces A: Physicochemical and Engineering Aspects, 241 (2004) 27-34.

[17] K. Morishige, N. Tateishi, F. Hirose, K. Aramaki, Change in Desorption Mechanism from Pore Blocking to Cavitation with Temperature for Nitrogen in Ordered Silica with Cagelike Pores, Langmuir, 22 (2006) 9920-9924.

[18] M. Kruk, M. Jaroniec, Argon adsorption at 77 K as a useful tool for the elucidation of pore connectivity in ordered materials with large cagelike mesopores, Chemistry of Materials, 15 (2003) 2942-2949.

[19] P.I. Ravikovitch, A. Vishnyakov, A.V. Neimark, M. Carrott, P.A. Russo, P.J. Carrott, Characterization of micro-mesoporous materials from nitrogen and toluene adsorption: Experiment and modeling, Langmuir, 22 (2006) 513-516.

[20] T.J. Bandosz, J. Jagiełło, J.A. Schwarz, A. Krzyzanowski, Effect of Surface Chemistry on Sorption of Water and Methanol on Activated Carbons, Langmuir, 12 (1996) 6480-6486.

[21] Salame, II, T.J. Bandosz, Effect of surface chemistry and pore structure on adsorption of water and CH3OH on activated carbons, in: D.D. Do (Ed.) Adsorption Science and Technology2000, pp. 61-65.

[22] J.K. Brennan, T.J. Bandosz, K.T. Thomson, K.E. Gubbins, Water in porous carbons, Colloids and Surfaces A: Physicochemical and Engineering Aspects, 187–188 (2001) 539-568.

[23] I.I. Salame, T.J. Bandosz, Interactions of water, methanol and diethyl ether molecules with the surface of oxidized activated carbon, Molecular Physics, 100 (2002) 2041-2048.

[24] V. Gun'ko, T.J. Bandosz, Heterogeneity of adsorption energy of water, methanol and diethyl ether on activated carbons: effect of porosity and surface chemistry, Physical Chemistry Chemical Physics, 5 (2003) 2096-2103.

[25] M. Thommes, C. Morlay, R. Ahmad, J.P. Joly, Assessing surface chemistry and pore structure of active carbons by a combination of physisorption (H2O, Ar, N-2, CO2), XPS and TPD-MS, Adsorption-Journal of the International Adsorption Society, 17 (2011) 653-661.

[26] M. Thommes, J. Morell, K.A. Cychosz, M. Fröba, Combining Nitrogen, Argon, and Water Adsorption for Advanced Characterization of Ordered Mesoporous Carbons (CMKs) and Periodic Mesoporous Organosilicas (PMOs), Langmuir, 29 (2013) 14893-14902.

[27] A. Michels, H. Wijker, H.K. Wijker, Isotherms of argon between 0°C and 150°C and pressures up to 2900 atmospheres, Physica, 15 (1949) 627-633.

[28] P.I. Ravikovitch, A. Vishnyakov, R. Russo, A.V. Neimark, Unified approach to pore size characterization of microporous carbonaceous materials from N2, Ar, and CO2 adsorption isotherms., Langmuir, 16 (2000) 2311-2320.

[29] B. Chen, J. Potoff, I. Siepmann, Monte Carlo Calculations for Alcohols and Their Mixtures with Alkanes. Transferable Potentials for Phase Equilibria. 5. United-Atom Description of Primary, Secondary, and Tertiary Alcohols., J. Phys. Chem. B., 105 (2001) 3093 - 3104.

[30] H.J.C. Berendsen, J.R. Grigera, T.P. Straatsma, The Missing Term in Effective Pair Potentials, Journal of Physical Chemistry B, 91 (1987) 6269-6271.

[31] W.A. Steele, The physical interaction of gases with crystalline solids: I. Gas-solid energies and properties of isolated adsorbed atoms, Surface Science, 36 (1973) 317-352.

[32] M.J. Bojan, W.A. Steele, Computer simulation of physisorption on a heterogeneous surface, Surface Science, 199 (1988) L395-L402.

[33] M.J. Bojan, W.A. Steele, Computer simulation of physical adsorption on stepped surfaces, Langmuir, 9 (1993) 2569-2575.

[34] C. Fan, L.F. Herrera, D.D. Do, D. Nicholson, New Method to Determine Surface Area and Its Energy Distribution for Nonporous Solids: A Computer Simulation and Experimental Study, Langmuir, 26 (2010) 5610-5623.

[35] R.D. Mountain, D. Thirumalai, Quantitative measure of efficiency of Monte Carlo simulations, Physica A (Amsterdam), 210 (1994) 453-460.

[36] H.E.A. Huitema, J.P. van der Eerden, Can Monte Carlo simulation describe dynamics? A test on Lennard-Jones systems, The Journal of Chemical Physics, 110 (1999) 3267-3274.

[37] A. Papadopoulou, F. Vanswol, U.M.B. Marconi, Pore-End Effects On Adsorption Hysteresis In Cylindrical And Slit-Like Pores, Journal of Chemical Physics, 97 (1992) 6942-6952.

[38] J. Jagiello, J. Kenvin, J. Olivier, A. Lupini, C. Contescu, Using a New Finite Slit Pore Model for NLDFT Analysis of Carbon Pore Structure, Adsorption Science & Technology, 29 (2011) 769-780.

[39] P.T.M. Nguyen, D.D. Do, D. Nicholson, On the Irreversibility of the Adsorption Isotherm in a Closed-End Pore, Langmuir, 29 (2013) 2927-2934.

[40] C. Fan, D.D. Do, D. Nicholson, On the Hysteresis of Argon Adsorption in a Uniform Closed End Slit Pore, Journal of Colloid and Interface Science, 405 (2013) 201-210.

[41] P.T.M. Nguyen, C. Fan, D.D. Do, D. Nicholson, On the Cavitation-Like Pore Blocking in Ink-Bottle Pore: Evolution of Hysteresis Loop with Neck Size, The Journal of Physical Chemistry C, 117 (2013) 5475-5484.

[42] Y. Zeng, C. Fan, D.D. Do, D. Nicholson, Evaporation from an Ink-Bottle Pore: Mechanisms of Adsorption and Desorption, Ind. Eng. Chem. Res., (2014).

[43] C. Fan, D.D. Do, D. Nicholson, Condensation and Evaporation in Capillaries with Nonuniform Cross Sections, Ind. Eng. Chem. Res., 52 (2013) 14304-14314.

[44] D.H. Everett, Adsorption hysteresis, Marcel Dekker, New York, 1967.

[45] A. Lotfi, J. Vrabec, J. Fischer, Vapour liquid equilibria of the Lennard-Jones fluid from the NpT plus test particle method, Molecular Physics, 76 (1992) 1319-1333.

[46] V.T. Nguyen, T. Horikawa, D.D. Do, D. Nicholson, On the relative strength of adsorption of gases on carbon surfaces with functional groups: fluid-fluid, fluid-graphite and fluid-functional group interactions, Carbon, 61 (2013) 551-557.

[47] D.D. Do, D. Nicholson, H.D. Do, On the Henry constant and isosteric heat at zero loading in gas phase adsorption, Journal of Colloid and Interface Science, 324 (2008) 15-24.

[48] V.T. Nguyen, D.D. Do, D. Nicholson, A new molecular model for water adsorption on graphitized carbon black, Carbon, 66 (2014) 629-636.

- Improved pore model for connectivity and functional group
- All hysteresis loops can be described by the new improved model
- New molecular model of carbon-functional group for polar adsorbates
- Importance of temperature in the characterization with adsorption isotherm